THE ASTRONOMICAL JOURNAL, 115:1617–1633, 1998 April

THE PRE–MAIN-SEQUENCE ECLIPSING BINARY TY CORONAE AUSTRALIS: PRECISE STELLAR DIMENSIONS AND TESTS OF EVOLUTIONARY MODELS

BRIAN W. CASEY AND ROBERT D. MATHIEU
Department of Astronomy, University of Wisconsin, 475 North Charter Street, Madison, WI 53706-1582; mathieu@astro.wisc.edu
LUIZ PAULO R. VAZ
Departamento de Física, Instituto de Ciências Exatas, Universidade Federal de Minas Gerais, C.P. 702, 30161-970 Belo Horizonte, MG, Brazil; lpv@fisica.ufmg.br
JOHANNES ANDERSEN
Astronomical Observatory, Niels Bohr Institute for Astronomy, Physics, and Geophysics, Juliane Maries Vej 30, DK-2100 Copenhagen Ø, Denmark; ja@astro.ku.dk
AND
NICHOLAS B. SUNTZEFF
Cerro Tololo Inter-American Observatory, National Optical Astronomy Observatories,[1] Casilla 603, La Serena, Chile; nick@ctio.noao.edu
Received 1997 May 20; revised 1997 November 18

ABSTRACT

We analyze new photometric data for the Herbig Be eclipsing binary TY CrA, which securely reveal the secondary eclipse, ~0.03 mag deep in *y*. From the light-curve solution and our previous spectroscopic data, absolute dimensions of the primary and secondary stars are derived. The masses are found to be $M_1 = 3.16 \pm 0.02\ M_\odot$ and $M_2 = 1.64 \pm 0.01\ M_\odot$, the radii are $R_1 = 1.80 \pm 0.10\ R_\odot$ and $R_2 = 2.08 \pm 0.14\ R_\odot$, the luminosities are $L_1 = 67 \pm 12\ L_\odot$ and $L_2 = 2.4 \pm 0.8\ L_\odot$, and the effective temperatures are $T_1 = 12{,}000 \pm 500$ K and $T_2 = 4900 \pm 400$ K. Here the uncertainties represent high-confidence limits, not standard deviations. The secondary star is a pre–main-sequence star located at the base of the Hayashi tracks. As such, it is the least evolved star with a dynamically measured mass. Given higher effective temperatures for the primary (e.g., 12,500 K), the solar-composition 1.64 $M_\odot$ evolutionary tracks of Swenson et al., Claret, and D'Antona & Mazzitelli are all consistent with the properties of the TY CrA secondary and suggest an age of order 3 Myr. The radius and projected rotational velocity of the secondary star are consistent with synchronous rotation. The primary star is located near the zero-age main sequence, which, for solar compositions, is consistent with an age of 3 Myr. However, the primary star is not well represented by any of the 3.16 $M_\odot$ evolutionary models, which predict somewhat higher effective temperatures than observed.

Key words: binaries: eclipsing — stars: evolution — stars: individual (TY Coronae Australis)

1. INTRODUCTION

The most fundamental parameter of a star is its mass, which determines almost everything about its birth, life, and death. Arguably, the second most important stellar parameter is radius, which is a sensitive indicator of the star's current evolutionary status. These stellar properties are uniquely provided together by the study of double-lined eclipsing binary stars, which have formed a foundation for observational tests of post–main-sequence stellar evolutionary theory (see review by Andersen 1991).

In contrast, pre–main-sequence (PMS) evolutionary theory remains largely unconstrained by measures of stellar masses and radii. To date, EK Cep has provided the youngest solar-mass star for which precise dimensions have been derived. The 2.0 $M_\odot$ primary lies on the main sequence, but the 1.12 $M_\odot$ secondary of EK Cep is PMS (Popper 1987; Claret, Giménez, & Martín 1995; Martín & Rebolo 1993). However, with an age of about 20 Myr, the secondary lies very near the main sequence and places very little constraint on PMS evolutionary tracks. In another study, Ghez et al. (1995) used speckle observations of T Tauri binaries to derive a mean system mass of 1.7 $M_\odot$. This measurement represents important dynamical evidence that T Tauri stars are near–solar-mass stars. However, no individual stellar masses have yet been derived from this sample.

The double-lined eclipsing binary TY CrA may thus provide an important datum to constrain PMS evolutionary theory. The orbital elements of TY CrA are well determined. Primary radial velocities and single-lined orbital solutions have been presented by Casey et al. (1993, hereafter Paper I) and Lagrange, Corporon, & Bouvier (1993). They found the orbit of the primary to be circular, with a period of 2.88878 days. Both Casey et al. and Lagrange et al. also noted the unusual narrowness of the primary spectral lines, corresponding to a (subsynchronous) projected rotational velocity of $v \sin i < 10$ km s^{-1}. Spectral lines of the secondary star, including Li I λ6708, indicative of youth, were identified by Corporon, Lagrange, & Bouvier (1994) and Casey et al. (1995, hereafter Paper II). These lines were used to derive a double-lined orbital solution, thus providing the secondary-to-primary mass ratio of $M_2/M_1 = 0.52$. The secondary of TY CrA is still early in the PMS stage (Paper II), with an age of a few million years. TY CrA also contains a tertiary star in a wider orbit about the close primary-secondary pair (Paper II; Corporon, Lagrange, & Beust 1996), and the whole system is embedded in a bright reflection nebula.

[1] The National Optical Astronomy Observatories are operated by the Association of Universities for Research in Astronomy, Inc., under cooperative agreement with the National Science Foundation.

Primary eclipses from the close binary were first detected by Kardopolov, Sahanionok, & Philipjev (1981). Vitrichenko & Shevchenko (1995, hereafter VS) reported a marginal detection (0.029 ± 0.011 mag deep in V) of the secondary eclipse at a phase of 0.5. From the V light curve, VS derived stellar radii of $R_1 = R_2 = 1.8 \pm 0.3\ R_\odot$ and noted long-term variations in the out-of-eclipse brightness of the TY CrA system. They concluded that both the primary and secondary are on the zero-age main sequence, with the secondary's large radius attributed to a dust shell.

Here we extend these previous studies with a detailed analysis of the photometric light curve, which, when combined with the spectroscopic orbital elements, allows us to derive precise masses and radii for the primary and secondary stars. We then compare these and other stellar parameters with the predictions of recent theoretical PMS stellar models. We first discuss the photometric data (§ 2.1), including a description of two sources of light in addition to that from the eclipsing pair (§ 2.2). We then derive the primary star's effective temperature (§ 3). Section 4.1 presents the light curves and briefly discusses brightness variations that are not due to the eclipses. In § 5, we derive the ephemeris and discuss the impact of the tertiary star on the observed times of minima. Section 6 describes our light-curve model, the input parameters, and the resulting absolute dimensions for the primary and secondary stars. We discuss these results as they relate to both previous observations and theoretical PMS evolutionary models in § 7. The reader who is not interested in the technical details may wish to skip directly to this section. Finally, § 8 summarizes our results.

2. PHOTOMETRY

2.1. *Overview*

TY CrA was observed in the *uvbyβ* photometric system with the Danish Strömgren Automatic Telescope (SAT; Nielsen, Nørregaard, & Olsen 1987) at the European Southern Observatory, La Silla, Chile. Observations were made on 22 nights in 1989 (covering seven orbital cycles), 14 nights in 1992 (four cycles), 19 nights in 1993 (six cycles), and 32 nights in 1994 (11 cycles). A total of 656, 134, 367, and 586 *uvby* observations were made, respectively. Each observation was made with a 17″ diameter diaphragm and was accompanied by a sky background measurement taken at a fixed position approximately 1.′5 away from the star. HD 176423 and HD 176497 were used as comparison stars and found to be constant within the observational accuracy throughout the observing periods. The mean errors of a magnitude difference between the comparison stars are 0.009 mag in u, 0.007 mag in v and b, and 0.006 mag in y.

The stars observed and summaries of our photometry are listed in Table 1. All indexes are from the 1994 observations except β, which is from the 1993 observations. The errors listed are internal rms errors. The indexes for TY CrA are listed both before and after correction for nebular contamination of the photometry (see § 2.2). Further details of these photometric observations are presented in Vaz et al. (1998). The data will be available in electronic form at the CDS.

2.2. *Stellar and Nebular Light Sources*

Our photometric measurements contain contributions from at least four different light sources. The light from the two stars in the close binary is of principal interest here. The unresolved tertiary star does not participate in the eclipses, but contributes to the measured fluxes. Finally, TY CrA and HD 176386 (1.′1 southwest of TY CrA) illuminate the reflection nebula NGC 6726/6727, whose light is a significant contributor to the photometric measurements.

To address the nebular contamination, *UBVRI* CCD images (13.′5 square) were kindly obtained by A. Layden on the Cerro Tololo Inter-American Observatory 0.91 m telescope in 1994 June. These images show substantial nebular contamination within our diaphragm at TY CrA. However, the position of our background measurements—60″ north and 60″ east of TY CrA— is fully outside the nebulosity.

In order to investigate the amount of nebular contamination, we also took measurements of TY CrA with the SAT using 13″ and 7″ diaphragms during five nights of exceptionally good seeing (better than 1″). These measurements are presented in Table 2. They are given as magnitude differences with respect to our comparison star HD 176423, which was measured with the 17″ diaphragm throughout the observations and found to be constant. Because the brightness of the TY CrA system is variable (see § 4.1), we restricted our analysis of nebular contamination to only those 17″ measurements that were taken at the same phase and overall light level as the smaller diaphragm measurements. The magnitude differences listed for the 17″ diaphragm in Table 2 are for this restricted data set of 39 observations, rather than the full set of observations.

Note that the color indexes (rightmost three columns of Table 2) become bluer with larger diaphragms, consistent with continued contamination from scattered light out to at least 8.″5 radius. Background contributions inside annuli limited by the different diaphragms, given as fluxes relative to HD 176423, are listed in Table 2 as B_{13-7} and B_{17-13}. Since the areas of these annuli are equal, it is immediately evident that the contribution of the nebular background is larger closer to TY CrA.

In order to determine the nebular contribution to our photometry, we needed to estimate the nebular contribu-

TABLE 1

OBSERVED STARS

Star	R.A. (B1950.0)	Decl. (B1950.0)	V	$b-y$	m_1	c_1	β
TY CrA:							
Uncorrected.....	18 58 18.55	−36 56 51.9	9.299(7)	0.407(5)	−0.004(13)	0.778(11)	2.783(1)
Corrected.....			9.65	0.45	−0.01	0.79	2.78
HD 176423	18 58 28.48	−36 44 11.9	9.017(6)	0.210(4)	0.150(7)	0.917(11)	2.849(3)
HD 176497	18 58 45.38	−36 26 02.2	8.377(8)	0.093(7)	0.161(4)	0.943(2)	2.865(1)

NOTES.—HD 176423 and HD 176497 are photometric comparison stars. The errors listed are internal rms errors. The indexes for TY CrA are listed both before and after correcting for nebular contamination of the photometry (see § 2.2). Units of right ascension are hours, minutes, and seconds, and units of declination are degrees, arcminutes, and arcseconds.

TABLE 2

NEBULAR CONTAMINATION

Parameter	y	b	v	u	$u-v$	$v-b$	$b-y$
Magnitude differences:[a]							
7″	0.524(7)	0.744(8)	0.790(9)	0.678(19)	−0.112(21)	0.046(12)	0.220(11)
13″	0.375(9)	0.577(7)	0.607(9)	0.474(18)	−0.133(20)	0.030(11)	0.202(11)
17″	0.296(1)	0.490(2)	0.511(2)	0.376(3)	−0.135(3)	0.021(2)	0.194(2)
Annular fluxes:[b]							
B_{13-7}	0.091(7)	0.084(5)	0.089(6)	0.111(14)			
B_{17-13}	0.054(6)	0.049(4)	0.053(5)	0.061(11)			
Estimated nebular flux within 17″ radius:[c]							
B_0	0.192(12)	0.176(8)	0.188(10)	0.230(23)			
B_l	0.214(16)	0.197(12)	0.209(14)	0.260(32)			
Nebula/Total	0.28(2)	0.31(2)	0.33(2)	0.36(4)			

[a] Magnitude differences between TY CrA (observed with the indicated diaphragm) and the comparison star HD 176423 (observed with the 17″ diaphragm). For the 7″ and 13″ diaphragms, the measurements are the average of five observations; for 17″ there are 39 observations.

[b] Fluxes within 7″–13″ and 13″–17″ annuli, relative to HD 176423. Note areas of both annuli are the same.

[c] B_0 is a minimum nebular flux, calculated assuming that the nebular light inside 7″ is constant at the B_{13-7} level. B_l is an estimation assuming that the nebular light increases linearly from 17″ to the center of the diaphragm. B_0 and B_l are relative to HD 176423. The ratio Nebula/Total is the fraction of the observed light (within the 17″ diaphragm) that is from the reflection nebula, based on the B_l estimation. All quoted uncertainties include only internal errors.

tion within the 7″ diaphragm (the contributions outside 7″ were directly measured, presuming that the stellar light was confined within the 7″ diaphragm). First, a lower limit was obtained by assuming that the nebular light level within 7″ remained constant at the level measured in the 7″–13″ annulus (B_{13-7} in Table 2). This lower limit is given as B_0 (again as a flux relative to the comparison star HD 176423) in Table 2 for each color.

The nebular contribution is likely greater than this lower limit, because it is probable that the background continues to increase in brightness closer to TY CrA. A second estimate of the nebular contamination was calculated by assuming that the nebular intensity increases linearly from the edge of the largest diaphragm to the center of the smallest one. This linear model (B_l in Table 2) yields nebular contamination results that are 11% (y) to 13% (u) larger than our lower limits.

These results were confirmed using the CCD images. We used IRAF to perform aperture photometry on the V image obtained in 1994 June. The resulting relative intensities of the annuli, B_{17-13} and B_{13-7}, are consistent with those derived from the SAT measurements. We also attempted to fit the stellar point-spread functon in order to subtract TY CrA and obtain a direct measurement of the underlying nebulosity. However, the large luminosity ratio between the stellar and nebular light precluded a measurement with adequate precision.

According to the linear model for the nebular contamination, we find that the nebulosity contributes from 28% to 36% of the total flux in our measurements of TY CrA, with greater contamination in bluer filters (see Table 2). These measures of the nebular contamination are somewhat model dependent. As such, we have chosen not to correct the light curves presented in Figures 1 and 2 below. However, we include in Table 1 the corrected photometric indexes for TY CrA, and we incorporate corrections for the nebular light in our light-curve analysis.

Our corrected values of V, $b-y$, and m_1 are consistent with the values $V = 9.73 \pm 0.08$, $b-y = 0.443 \pm 0.012$, and $m_1 = 0.004 \pm 0.020$ given by Marraco & Rydgren (1981), who also corrected for nebular contamination. Our values of c_1 and β are somewhat less consistent with their $c_1 = 0.726 \pm 0.027$ and $\beta = 2.807 \pm 0.010$. Our values of both c_1 and β imply a slightly lower effective temperature than those of Marraco & Rydgren (1981), as discussed in the next section.

3. PRIMARY TEMPERATURE

The effective temperature of the primary star was calibrated using the standard Strömgren indexes. Specifically, we calibrated the primary effective temperature based on $[u-b]$, where

$$[u-b] \equiv 2m_1 + c_1 + A(b-y), \tag{1}$$

with

$$A = 2 - \frac{E(u-b)}{E(b-y)}. \tag{2}$$

For A, which varies depending on the region, we adopted a value of 0.40.

By linear interpolation of $[u-b]$ in Table 2 of Davis & Shobbrook (1977), we find a primary effective temperature of 12,040 K. Using the calibration of Napiwotzki, Schönberner, & Wenske (1993), we find a temperature of 11,960 K.

Shobbrook (1976) reported A-values of 0.32, 0.40, and 0.48 for the Upper Cen, Sco OB1, and h and χ Per regions, respectively. Variations of 0.08 in A result in temperature ranges of about 11,800–12,300 K for the Davis & Shobbrook calibrations and 11,750–12,460 K for Napiwotzki et al.

For the standard indexes from Marraco & Rydgren (1981) and $A = 0.40$, we derived primary temperatures of 12,350 and 12,270 K using the Davis & Shobbrook and Napiwotzki et al. calibrations, respectively. For A ranging from 0.32 to 0.48, the derived primary temperature ranges between 12,100 and 12,600 K.

These primary temperatures are all based on color indexes that have been corrected for nebular contamination. Temperatures derived with the uncorrected indexes are about 200 K higher than those from corrected values. The corrected indexes still include the contamination of the secondary and tertiary stars. However, light from the primary dominates the stellar contribution to our photom-

etry [e.g., $l_1/(l_2 + l_3) > 10$; Paper II]. The effective temperatures derived above should closely correspond to that of the primary. Based on these calibrations, we estimate a primary temperature of $T_1 = 12{,}000 \pm 500$ K.

Spectral types reported for TY CrA in the literature range from B2 (SAO Catalog, 1966) to A5 (Hillenbrand et al. 1992; but see Paper I). Determinations based on examination of the primary star in some detail agree on a spectral type of B8 with an uncertainty of one subclass (B7, Lagrange et al. 1993; B8–B9, Paper I; B9, Herbig & Rao 1972; Bibo, Thé, & Dawanas 1992 also find a spectral type of B8 based on broadband colors). Temperatures for normal stars with spectral types between B9 and B7 range between 10,350 and 12,800 K, from the calibration of Straizys & Kuriliene (1981). Popper (1980) lists temperatures of 10,350–12,940 K for spectral types of B9–B7. Thus, the line spectrum of TY CrA is consistent with our effective temperature inferred from its intermediate-band colors. In addition to providing corroboration, this result supports a photospheric origin for the peculiarly narrow lines.

4. PHOTOMETRIC BEHAVIOR

4.1. *Eclipse Light Curve*

We used the combined 1992 and 1993 data set as our standard TY CrA light curve. Our reasons are twofold. First, TY CrA exhibits photometric variations on both orbital and longer timescales that are not associated with eclipses. The 1992 and 1993 data are relatively free of such variability while, during the 1994 observations, TY CrA was highly variable. Second, because of photometric conditions the precision of the 1989 data is substantially poorer, and their inclusion would degrade the light curve.

The 1992–1993 y light curve of TY CrA is shown in Figure 1. Note the deep ($\sim$0.4 mag) primary eclipse and the shallow ($\sim$0.03 mag) secondary eclipse. Both eclipses are partial. The light curve also exhibits a strong reflection effect (the increase in brightness between primary and secondary eclipse), which is typical of close binary systems.

The color index curves in $u - v$, $v - b$, and $b - y$ for TY CrA are shown in Figure 2. The larger measurement errors in u and v are apparent in the scatter of the $u - v$ index curve. The expected blueing in the secondary eclipse (a result of decreasing the contribution of the red secondary relative to the blue primary) can be seen at phase 0.5 in the $b - y$ and $v - b$ curves. Note that the primary eclipse *also* exhibits a blueing in color. During primary eclipse, the secondary star makes a relatively larger contribution to the combined light. However, the nebular contamination discussed in § 2.2 also increases relative to the primary. Since the blue nebula contributes more light than the faint red secondary and tertiary stars, the light curve becomes bluer in the primary eclipse.

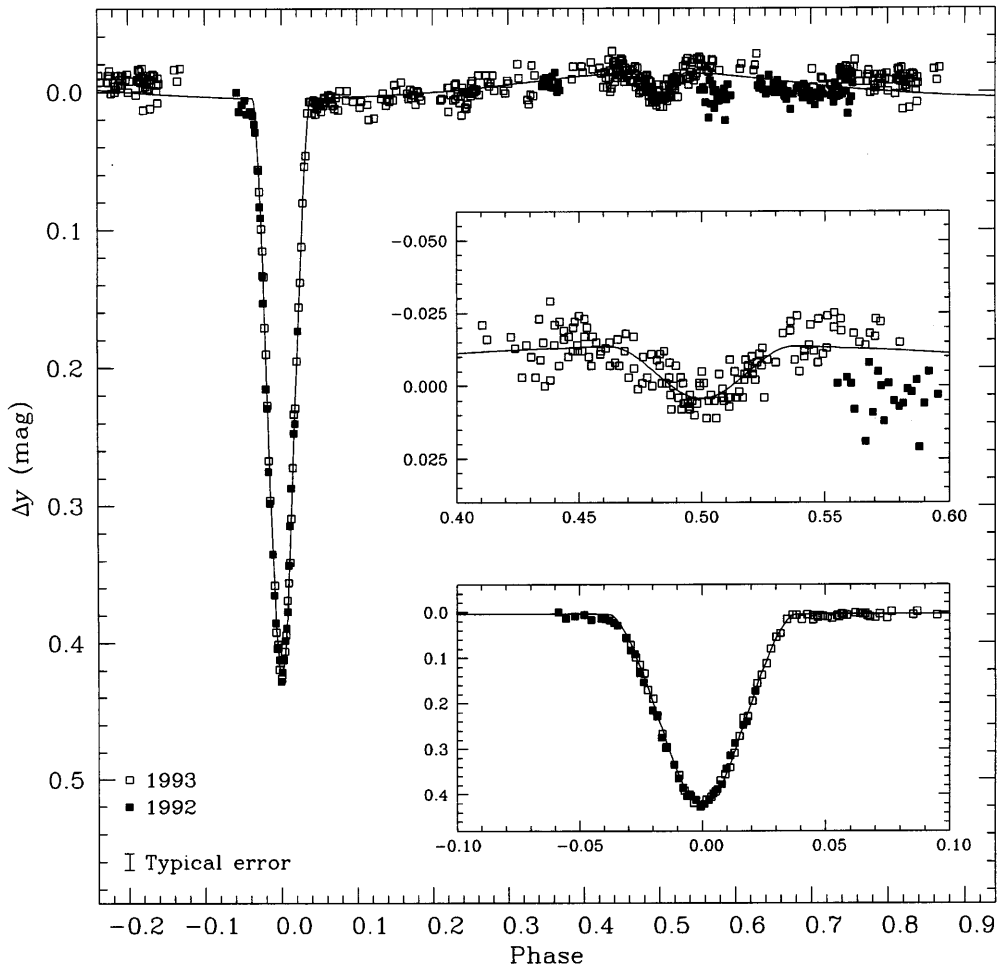

FIG. 1.—Light curve in y for TY CrA during 1992 and 1993. The phase is from the ephemeris given in § 5. The magnitude is the offset from y measured near quadrature. The typical error of 0.006 mag is indicated. Note the shallow secondary eclipse at phase 0.5 and the strong reflection effect. The inset figures expand the regions around the primary and secondary eclipses.

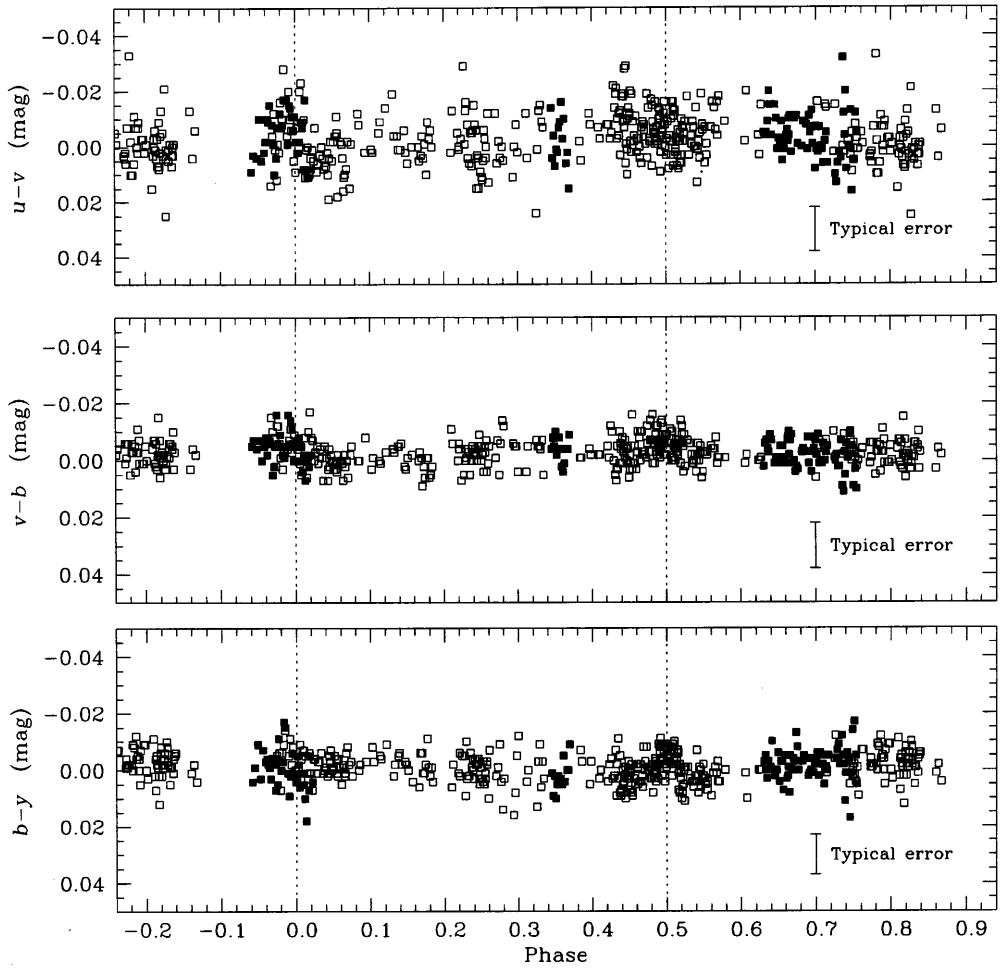

FIG. 2.—Light curves in $u - v$, $v - b$, and $b - y$ for TY CrA during 1992 and 1993. Symbols are as in Fig. 1. Dotted lines are drawn at phases 0.0 (primary eclipse) and 0.5 (secondary eclipse). TY CrA becomes slightly bluer during (secondary) eclipse of the pre–main-sequence companion. The system also becomes slightly bluer during primary eclipse, indicative of a flux contribution from the reflection nebula.

4.2. *Non-Eclipse Photometric Variations*

We find TY CrA to vary photometrically on timescales from days to years. These variations are not evidently related to eclipse phenomena, although in some cases they are phased with the binary orbit. We characterize these variations here in order of increasing timescale.

During 1993, we see no evidence for photometric variations unrelated to the eclipses. For example, a linear least-squares fit to the region between phases 0.1 and 0.4 yields an rms of 0.007 mag, close to the observed measurement error of 0.005 mag derived from the comparison-star observations. Similarly, the scatter of the 1993 data about our light-curve solution (§ 6) is only 0.007 mag.

On the other hand, the observations in 1994 exhibit substantial photometric variations (Vaz et al. 1998). These variations can be seen in Figure 3, where we plot the first and second quadratures of the y light curves from each year of observation. Comparison of the 1993 and 1994 data clearly reveals the increase in photometric variability in 1994. Occasionally, the timescale of the variability is less than 1 day. A linkage between this variability and orbital phase is not obvious.

Data from 1992 and 1993 reveal a photometric variation that is linked to orbital phase. In particular, near phase 0.7 the 1992 observations lie about 0.015 mag fainter than the 1993 observations (see Fig. 1). Lower precision data show this feature to extend to phase 0.55 during one cycle. This feature was repeated on three nights of observing during three sequential orbital cycles. Invoking a systemic shift of 0.015 mag at all phases in order to explain the observations near phase 0.7 is inconsistent with observations at primary eclipse and at phase 0.4, where the 1992 and 1993 photometry agree well. Indeed, observations of a 1992 primary eclipse showing no shift in brightness were obtained between two sets of observations near phase 0.7 that showed the decreased brightness. This decrease is not evident in the 1989, 1993, or 1994 data, although none of these years provided numerous precise, stable photometric measurements at second quadrature.

Finally, the observations show systemic variability over timescales of years. For example, the 1989 observations show TY CrA to be consistently 0.10 mag fainter than in 1993 (Fig. 3). Similarly, our 1994 observations are on average about 0.03 mag fainter than those of 1993. The same comparison stars were used in all sets of observations, and the magnitude difference between them remained constant and at the same level throughout.

VS also reported large ($\sim$0.3 mag) variations in the out-of-eclipse brightness of TY CrA over a period of about 5000 days. Measurements in the literature (e.g., Herbst et al. 1994) similarly suggest substantial variation. However, analyses of long-term changes using literature data are

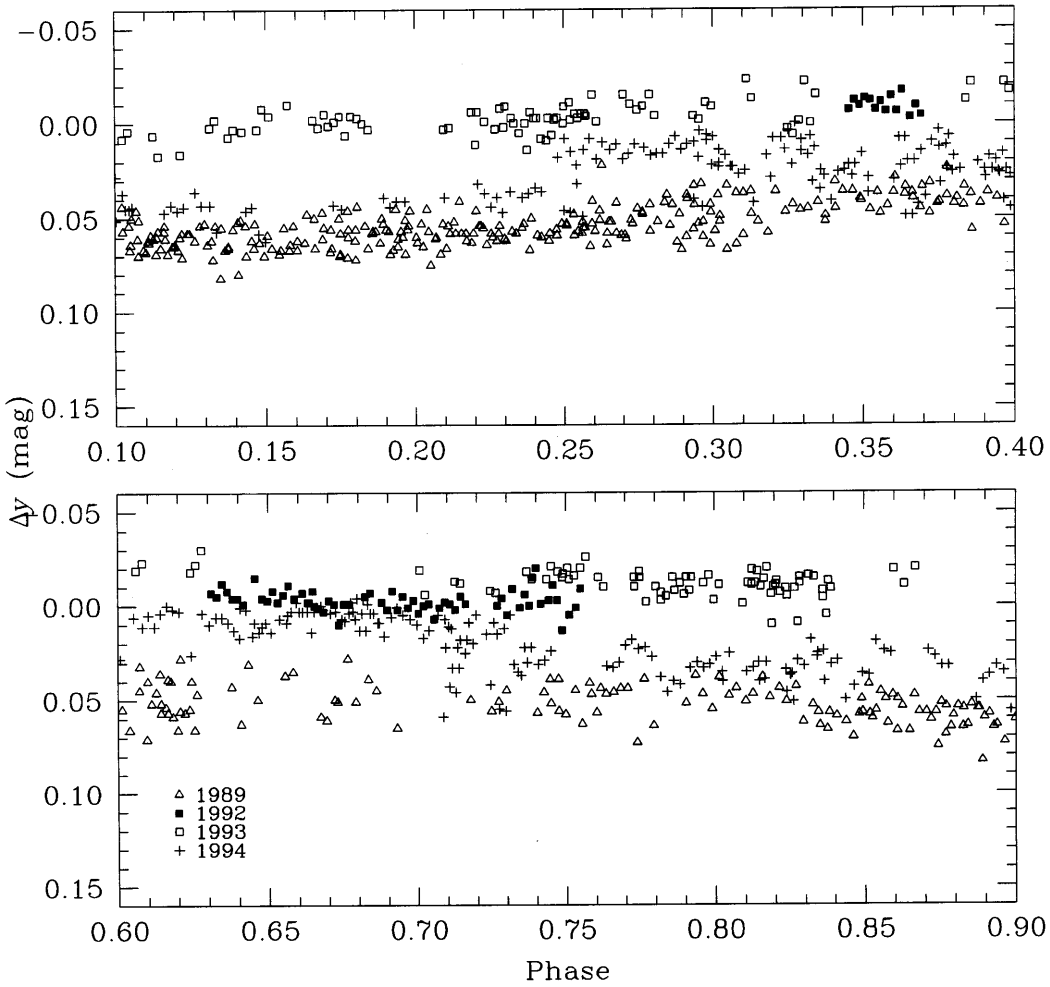

FIG. 3.—The y light curves of TY CrA at first (*top*) and second (*bottom*) quadratures in four different years. Magnitudes are plotted with respect to quadrature in the 1993 data. Note the large brightness variations, both between seasons and within the 1994 season.

complicated by differing nebular contamination due to varying diaphragm size.

The non-eclipse photometric variability is much less evident in the color index curves. In Figure 4, we plot the color index $b - y$ as a function of orbital phase at the first and second quadratures for each year of observation. Both long- and short-term variations, including the feature at phase 0.7 seen in the 1992 data, are nearly gray.

The cause of these noneclipse variations in the TY CrA light curve remains to be found. Vaz et al. (1998) find in the 1994 data evidence for reddening with a large value of total to selective extinction. They thus suggest that the light variations are due to variable dust obscuration, plausibly linked to the circumbinary material inferred from mid- and far-infrared excesses (Paper I; Bibo et al. 1992). An external origin of at least some of the variations is also consistent with our observation that the depth of the primary eclipse was unchanged from 1989 to 1994.

4.3. *Primary Minimum Asymmetry*

The primary minimum has a small asymmetry, with its descending branch being systematically brighter and bluer than the ascending branch. The feature was first seen in the residuals around our light-curve model, which was forced to produce symmetric eclipses, but is hardly discernable in Figure 1. It can also be seen in a plot of $u - b$ color versus phase folded about phase 0.0 (Casey 1996). The asymmetry is also present in our 1989 and 1994 data, and so apparently has been stable for at least 5 years.

5. EPHEMERIS

5.1. *Computation of Ephemeris*

Using data from all 4 years, we have measured 11 times of eclipse minima (seven primary and four secondary). Measurements of the times of primary minimum were made by applying the method of Kwee & van Woerden (1956) to all four colors, confirming the results with second-order polynomial fits. The mean of the four measures was adopted, with an uncertainty derived from their rms dispersion. Our results are given in Table 3.

Because of the shallowness of the secondary eclipse, this approach succeeded in all four colors only for the 1994 secondary eclipse. For the 1992 secondary eclipse, only the y curve produced a successful measurement, and for the second secondary eclipse observed in 1993, only the b and y light curves could be used. Finally, for the first secondary eclipse of 1993 both methods failed in all four colors. For this eclipse, the time of minimum and its uncertainty were estimated graphically. Uncertainties were computed from the interagreement of measurements from different colors when available, and otherwise from the internal errors.

We use only the primary minima to obtain a measure of

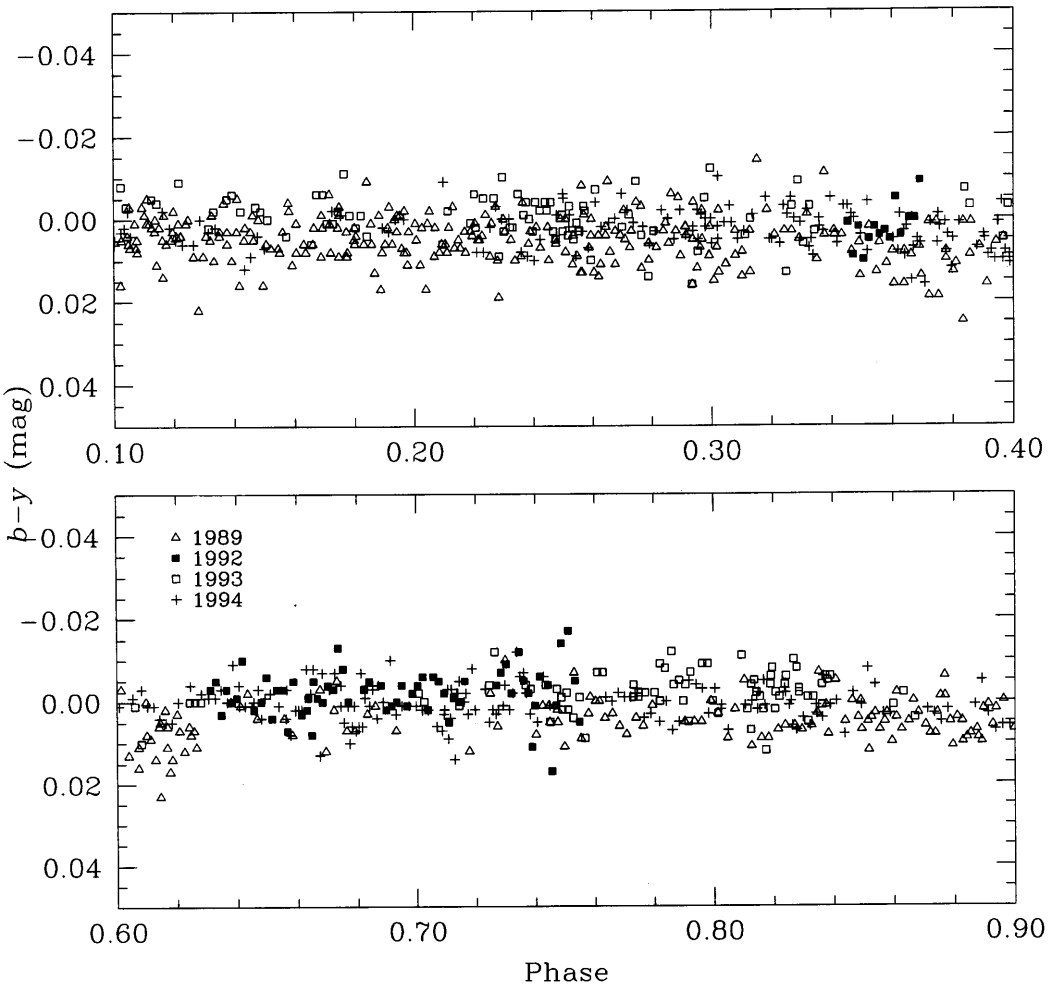

FIG. 4.—The $b - y$ light curves of TY CrA at first (*top*) and second (*bottom*) quadrature in four different years. The long-term time variability evident in each color (Fig. 3) is not present in the color indexes.

the orbital period. The Lafler & Kinman (1965) period-search method yields a period of $P = 2.888779 \pm 0.000013$ days. Alternatively, we find by linear least squares $P = 2.88878 \pm 0.00004$ days. Both determinations are in good agreement with the photometric determinations of Kardopolov et al. (1981), who quote $P = 2.888777$ days (without an error estimate), and VS, who report $P = 2.888779 \pm 0.000001$ days. These periods also agree well with the period determined spectroscopically in Paper II, $P = 2.888776 \pm 0.000006$ days.

TABLE 3

TIMES OF ECLIPSE MINIMA

Season	HJD (2,440,000+)	Eclipse Type	$O-C$ (days)	Cycle	Phase
1989.....	7,694.7971(9)	Primary	0.0029	−638	0.9989(29)
	7,700.5740(5)	Primary	0.0036	−636	0.9986(29)
	7,710.68(8)[a]	Secondary	−0.0087	−632	0.4970(278)
1992.....	8,783.8703(13)	Primary	−0.0006	−261	0.0001(13)
1993.....	9,153.6302(4)	Primary	0.0032	−133	0.9988(7)
	9,160.85(2)[b]	Secondary	−0.0057	−130	0.4980(70)
	9,163.74(1)[c]	Secondary	−0.0045	−129	0.4984(35)
1994.....	9,514.7310(3)	Primary	−0.0002	−8.0	0.9999(3)
	9,527.738(5)	Secondary	−0.0080	−3.5	0.5027(18)
	9,537.8412(8)	Primary	−0.0002	0.0	0.9999(4)
	9,543.6193(3)	Primary	−0.0007	2.0	0.0012(3)

NOTE.—$O-C$ values, cycle numbers, and phases are with respect to the ephemeris for primary minimum HJD 2,449,537.8414 + 2.888779E (see § 5).

[a] Only the y light curve could be used.

[b] Both the second-degree polynomial and Kwee & van Woerden 1956 methods failed. The time of minimum was estimated graphically.

[c] Only the b and y curves could be used.

We adopt the ephemeris

$$\text{Min I: HJD } 2{,}449{,}537.8414(8) + 2.888779(13)E\ ,$$

where E is the epoch number. In Table 3, we use this ephemeris to calculate the $O-C$ values listed and the phases of the observed times of secondary minima. All phases for the secondary eclipse are very close to 0.5, consistent with a circular orbit (Paper II).

5.2. *Influence of the Tertiary Star*

The $O-C$ values in Table 3 exhibit deviations significantly larger than the expected errors. These deviations are shown in Figure 5, where we plot $O-C$ versus Julian Date for the times of minimum. The implication is that the apparent period of the TY CrA binary has varied over the last 5 years. Some variation is expected, given the presence of the tertiary star. As the tertiary and primary-secondary pair orbit each other, the light-travel time from the binary changes, causing shifts in observed times of minimum. We suggest that the observed deviations in the $O-C$ values are due to this light-time effect.

These phase shifts complicate our combination of the 1992 and 1993 light curves. Corporon et al. (1996) have presented five different spectroscopic orbital solutions, which have periods ranging from 126 to 270 days. However, given the uncertainty of these solutions, and their inconsistency with our measured times of minima (see below), it seems premature to use them to correct for the influence of the tertiary. Instead, we adopt the period determined in the previous section for each of 1992 and 1993. Orbital phases are calculated for each season's data independently relative to the respective times of minima, after which the two seasons' data are combined. This procedure effectively corrects for the small phase shift (0.0013) between the two seasons.

While our data are insufficient to calculate orbital elements for the tertiary star, they do provide several significant limits. Specifically, a minimum period for the tertiary orbit may be calculated as a function of tertiary mass. We assume that the orbit of the tertiary-binary pair is coplanar with the primary-secondary orbit (thereby having an inclination angle of $\approx 90°$) and that the major axis of the tertiary orbit is along the line of sight. We also assume that the observed peak-to-peak $O-C$ deviation corresponds to the light-travel time across the major axis of the binary's orbit around the tertiary. With these assumptions, the *minimum* period of the tertiary-binary pair may be calculated as a function of tertiary mass. Changes in the tertiary orbit's orientation, or a major axis larger than indicated by the shifts in eclipse times, will produce longer periods for the tertiary-binary orbit.

The peak-to-peak deviation in times of primary minima that we observe is 0.004 days. Taking this value, the minimum period of the tertiary-binary orbit as a function of tertiary mass is shown by the solid curve in Figure 6.

In addition, the deviations in primary $O-C$ change sign twice between 1992 and 1994 (Table 3 and Fig. 5). Thus, tertiary-binary orbits much longer than about 2 yr are excluded by our data. Combining these two constraints results in a lower limit on the tertiary mass of about 0.6 $M_\odot$. Alternatively, in Paper II we estimated a tertiary mass of $2.4 \pm 0.5\ M_\odot$. This estimate, about twice the value found by Beust et al. (1997), is independent of any assumptions on the period of the outer orbit or the inclination between the two orbital planes. Such a tertiary mass corresponds to a lower limit on the period of the tertiary orbit of about 140 days.

Corporon et al. (1996) gave five different orbital solutions for the tertiary star based on radial velocity measurements. These solutions have periods between 126 and 270 days, seemingly consistent with the above limits. However, all the solutions have inclinations of about 20°—approaching per-

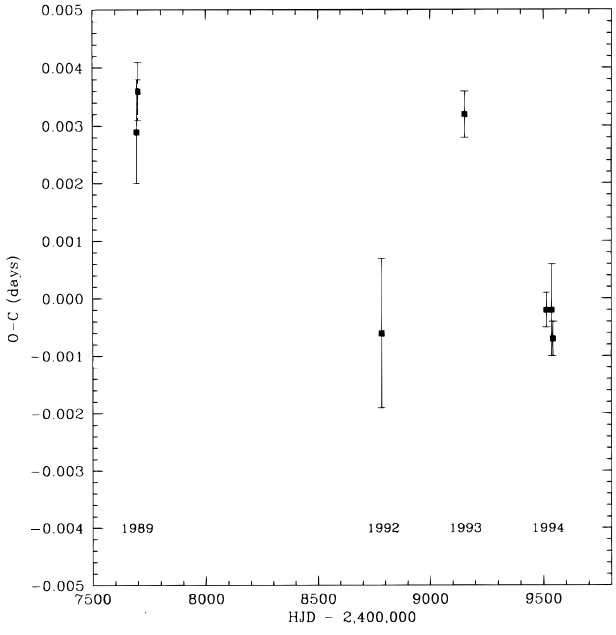

FIG. 5.—$O-C$ for times of primary minimum vs. date. Note the variations in observed times of minimum, likely caused by the orbit of the primary-secondary pair around the tertiary star.

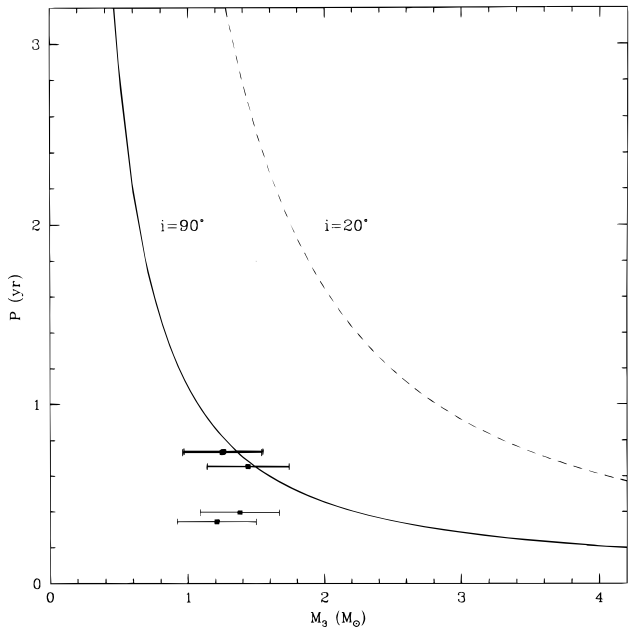

FIG. 6.—Minimum period of the tertiary-binary orbit as a function of tertiary mass, presuming a light-travel time across the major axis of 0.004 days. The solid curve represents the minimum period assuming the tertiary orbit is edge-on. The dashed curve corresponds to a tertiary orbit with an inclination of 20°, approaching perpendicular to the orbit of the binary. Squares represent the orbital solutions from Corporon, Lagrange, & Beust (1996), all of which have inclinations near 20°.

pendicular to the orbital plane of the binary. Such a low inclination significantly raises the minimum period as a function of tertiary mass derived from our observed $O-C$ deviations, as shown by the dashed curve in Figure 6. Also shown in Figure 6 (*squares*) are the tertiary masses and periods derived from the five suggested orbital solutions. These are not consistent with the lower limits on the orbital period derived from our $O-C$ deviations assuming $i = 20°$. Similarly, our light-travel time data provide a direct measure of the *minimum* value of $a \sin i$ for the orbit of the center of gravity of the inner binary around that of the entire system. We find $a \sin i \geq 5.0 \times 10^7$ km, or $a \sin i \geq 0.34$ AU, while the tertiary orbits proposed by Corporon et al. (1996) all imply $a \sin i \leq 0.17$ AU for the inner binary. Indeed, the magnitude and even sign of the eclipse time variations are incompatible with the positions of the inner binary as computed from these orbits.

In summary, our observations of the light-travel time effects of the orbit of the eclipsing pair are in disagreement with the set of candidate orbits proposed by Corporon et al. (1996). We note that this discrepancy is of major importance for our understanding of the dynamics of the system, including the striking nonsynchronism of the primary star, since a highly inclined tertiary orbit forms the basis for the dynamical history of TY CrA developed by Beust et al. (1997). Additional measurements of the radial velocity of the third star and/or times of minimum of the eclipsing binary will be needed to determine well the period and dimensions of the outer orbit in the system.

6. LIGHT-CURVE ANALYSIS

6.1. *Light-Curve Model and Stellar Input Parameters*

We have restricted our modeling of the 1992–1993 light curve to the *y*-band data because (1) the secondary minimum is by far the best defined here, (2) our spectroscopic constraints on the luminosities of the secondary and tertiary stars are closest to the *y* band in wavelength, and (3) contamination by the blue nebular light is minimum. We have also excluded phases 0.55–0.80 from the 1992 data, which show non–eclipse-related light variations.

We have used a modified version of the Wilson-Devinney (WD) light-curve synthesis program (Wilson & Devinney 1971; Wilson 1993a, 1993b) to model the light curve of TY CrA. Several physical and practical modifications and improvements have been made to the 1993 version of the code; we refer the reader to the paper by Vaz, Andersen, & Rabello Soares (1995) for a detailed description and only mention those particularly relevant to the present analysis in what follows. In addition, the WD program requires several physical parameters other than the photometric elements to be determined in the analysis; the more important of these are also briefly discussed.

The spectroscopic analysis of Paper II provides several physical constraints. The mass ratio is $q = M_2/M_1 = 0.521 \pm 0.005$. The projected rotational velocity of the primary star is $v_1 \sin i \leq 10$ km s^{-1} (Paper I; Lagrange et al. 1993); in our models, we fixed v_1 at 10 km s^{-1}. The rotational velocity of the secondary ($v_2 \sin i = 32 \pm 3$ km s^{-1}; Paper II) is consistent with synchronous rotation, as expected theoretically, and synchronous rotation was assumed in all models.

The limb darkening of both stars was described using the linear square root parameterization given by Van Hamme (1993). The limb-darkening coefficients were calculated by bilinear interpolations using the current values of log g and $T_{\rm eff}$.

The gravity-brightening exponent was fixed at 1.0 for the primary star, as appropriate for stars with radiative envelopes (von Zeipel 1924). Lower values are expected for stars with convective atmospheres (Lucy 1967), such as the secondary component of TY CrA, and we have used the recent formulation (Alencar & Vaz 1997) based on detailed model atmosphere calculations (Nordlund & Vaz 1990 and references therein). We note that the resultant β-value for the secondary is $\sim$28% larger than Lucy's value.

The radiated flux of both stars is described by atmosphere model tables, updated relative to the original versions of the WD code. For the primary star we used those by Kurucz (1979), while tables based on the newer calculations of Buser & Kurucz (1992) were used for the cooler secondary.

The bolometric albedo for the primary was fixed at 1.0 (100% of the incident flux reradiated locally), as appropriate for radiative envelopes (Eddington 1926). The bolometric albedo for the convective secondary was left free to be adjusted in the solutions, starting from the value 0.5. Single reflection was considered in all of our solutions.

The light curve of TY CrA is affected by appreciable additional light from the tertiary star and the reflection nebula ("third light"). The original WD model parameterizes third light as a constant amount added to the total absolute flux from the eclipsing system. However, the total absolute flux from the eclipsing components changes from solution to solution as a result of changes in their sizes and relative temperatures, requiring adjustment of the absolute amount of third light for a fixed *relative* contribution. As our physical information constrains the amount of extra light relative to the eclipsing pair at a certain phase, we introduced the same parameter L_3 as defined in the WINK model (Wood 1971, 1972; Vaz 1984, 1986), which in the present case is equivalent to

$$L_3 = \frac{(l_3/L_2)[l_2/(l_1 + l_2)]_\phi + B_l 10^{0.4Q}}{1 - B_l 10^{0.4Q}}, \qquad (3)$$

where l_1, l_2, and l_3 are the stellar contributions, B_l is the light from the nebula, ϕ is a normalization phase, and Q is the magnitude at phase ϕ, taken from our photometry. The ratio l_3/l_2 is constrained from spectroscopy (Paper II) to be in the range 0.5–3.9 at 6400 Å (the region nearest *y* at which lines from both stars were observed); as it was also estimated that $M_3 > M_2$, we adopt a value $l_3/l_2 = 2.0$. The nebular contribution in the standard diaphragm used for the light-curve data is estimated from our photometry to be $B_l(y) = 0.2$ (Table 2 and § 2.1), adopting the linear model for the nebular light. Finally, the primary and secondary luminosities (l_1 and l_2) were taken from the most recent iteration of the solution.

6.2. *Solution Grid*

Our initial solution procedure involved differential least-squares corrections to seven parameters: inclination, secondary and primary temperatures, primary luminosity, secondary albedo, and both stellar surface gravitational pseudopotentials (effectively, stellar radii). In addition, the limb-darkening coefficients, normalization magnitude, third-light parameter (as affected by changing the luminosity ratio l_1/l_2), gravities, and primary $v_{\rm rot}/v_{\rm synch}$ were all

changed between successive runs of the WD program to always correspond to the solution of the previous iteration.

We achieved converged solutions for these free parameters, but we found that the solutions depended on their starting values. Investigation showed that the χ^2 surface does not have a single, well-defined minimum, and consequently we were required to map the surface. To achieve this, we computed light-curve solutions for a three-dimensional grid in primary temperature, secondary temperature, and secondary gravitational potential. The last effectively fixes the radius and luminosity of the secondary since, at the high inclination angle of TY CrA, the stellar masses change little between solutions. Given our derived primary temperature of 12,000 $\pm$ 500 K (§ 3), we chose initial grid points in primary temperature T_1 of 11,500, 12,000, and 12,500 K. Grid points for the secondary were spaced by 215 K in effective temperature and roughly 0.07 in log luminosity. The range of secondary grid points was extended until the light-curve solutions fitted poorly or the primary-to-secondary luminosity ratio deviated greatly from the spectroscopic constraint. The locations of the secondary grid points in log L–log $T_{\rm eff}$ space are shown in Figure 7.

For each point in the grid, we considered the solution to have converged when the corrections for each of the free parameters in the least-squares solution were both at least 3 times smaller than the corresponding errors and oscillating in subsequent iterations. The free parameters converged to values at well-defined minima. We examined each solution and found that rms deviations of greater than 0.0073 mag corresponded to clearly unacceptable systematic deviations between the theoretical and observed light curves. We thus conservatively adopt this criterion to restrict the domain of parameter space in which the TY CrA stars lie.

In Figure 7, we show contour plots of the rms statistic in the log L–log $T_{\rm eff}$ plane of the secondary star. Each panel corresponds to one of the adopted primary temperatures. The contours corresponding to the 0.0073 mag rms value are shown in bold. The goodness-of-fit surface is a valley in the secondary log L–log $T_{\rm eff}$ plane whose bottom runs approximately along an isoradius: for a given T_1, there exists a family of secondary solutions along a line of approximately constant secondary radius. The permitted regions for the secondary are similar for all primary temperatures.

Evidently, the light curve alone permits large ranges in effective temperature, luminosity, and radius for the primary and secondary stars of TY CrA. However, external observations further constrain these parameters. The constraint on the primary temperature from our Strömgren photometry has already been applied by our choice of primary temperatures for the grid. The other significant constraint is the primary-to-secondary bolometric luminosity ratio as a function of secondary temperature, which was determined spectroscopically in Paper II. As described there, the derived primary-to-secondary bolometric lumi-

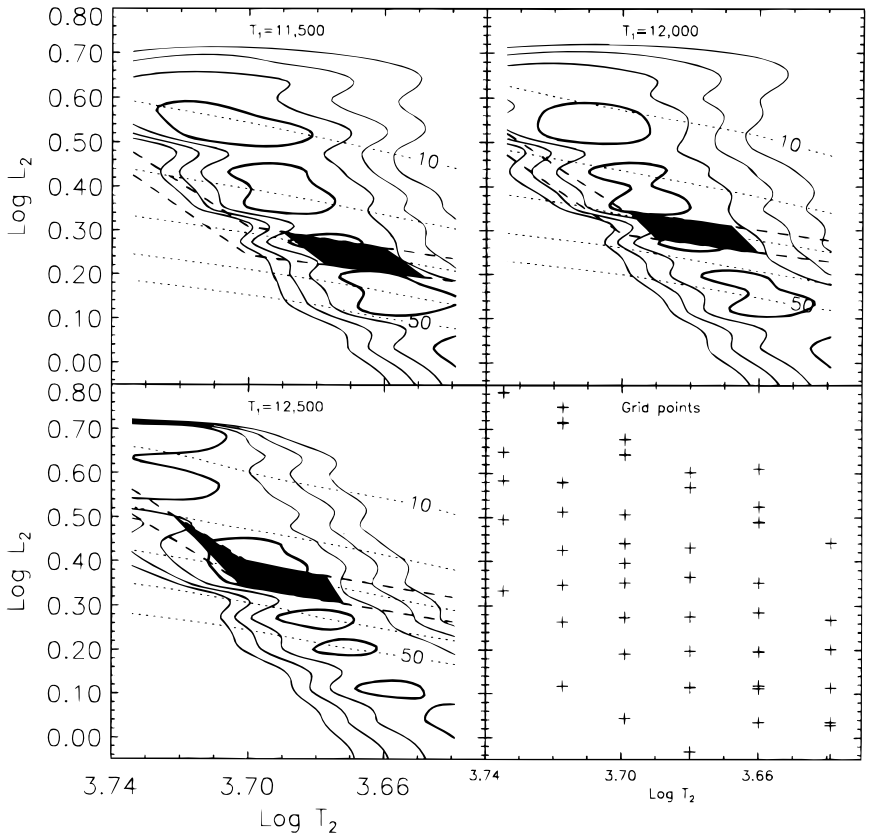

FIG. 7.—Goodness-of-fit surfaces in the L-$T_{\rm eff}$ plane of the secondary star. The contours map the rms about light-curve models for three primary effective temperatures, T_1. Contours are drawn at rms values of 0.00730, 0.00745, 0.00760, and 0.00775 mag. The bold contours at 0.00730 mag correspond to the maximum acceptable rms (see § 6.2). Note that acceptable solutions are distributed along a valley in the L-$T_{\rm eff}$ plane. Dotted lines are drawn for constant primary-to-secondary luminosity ratios between 10 and 50, in increments of 10. The dashed lines correspond to the primary-to-secondary luminosity ratio limits from Paper II. The shaded regions delimit solutions that are allowed by both the rms and luminosity ratio constraints. The bottom right panel shows the location of the model grid points used to generate the contours.

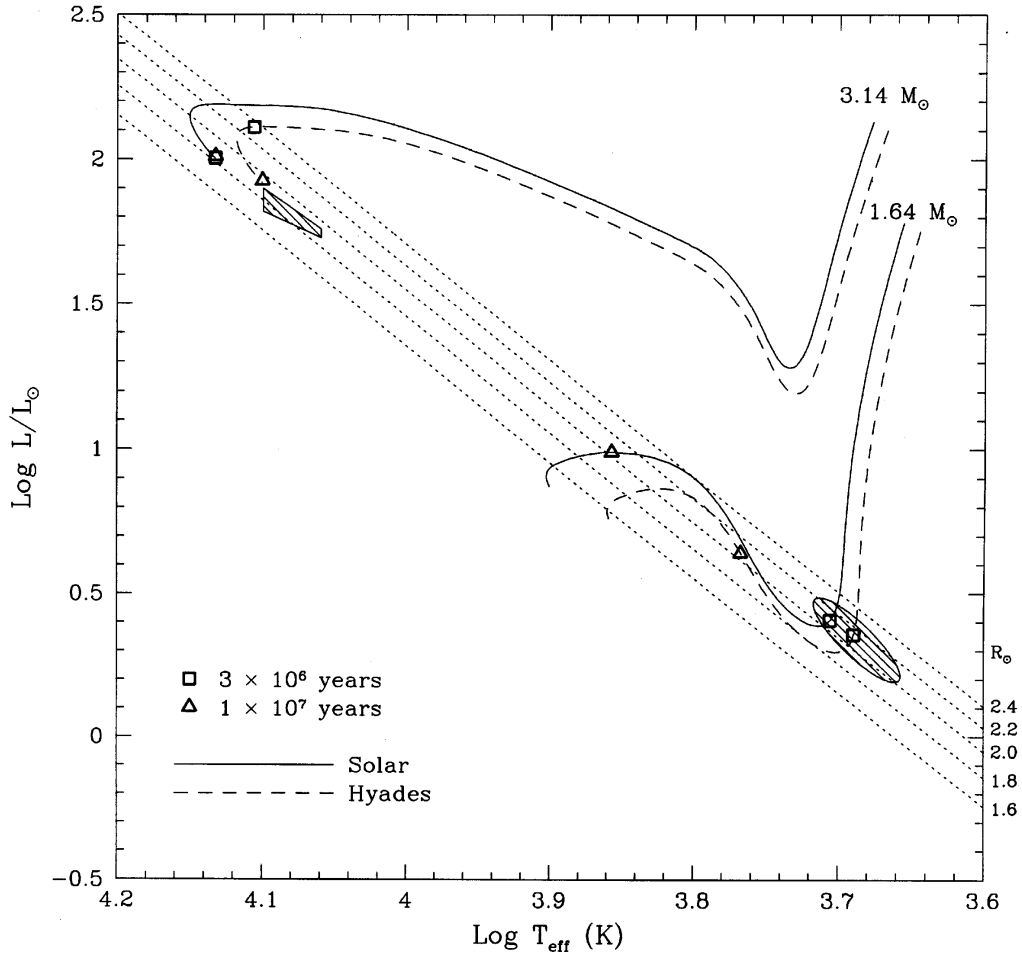

FIG. 8.—Location of TY CrA primary and secondary stars in the theoretical H-R diagram. The hatched regions designate high-confidence domains for the primary and secondary stars based on light-curve analyses (§ 6.2). Dotted lines are drawn at constant radii. Solid and dashed curves correspond to pre–main-sequence tracks of Swenson et al. (1994), calculated for the masses of the primary and secondary of TY CrA. Tracks for solar (*solid curve*) and Hyades (*dashed curve*) compositions are shown. Squares and triangles mark isochrone points at ages of 3 and 10 Myr, respectively.

nosity ratio depends on the tertiary temperature. In each panel of Figure 7, we show two dashed lines representing the secondary luminosity as a function of secondary temperature for tertiary spectral types F5 and K5. The secondary luminosity is constrained to lie between these lines.

For each primary temperature, we have shaded those regions in Figure 7 within which fall light-curve solutions that both fit the observed light curve *and* satisfy the bolometric luminosity ratio constraint.[2] The union of these shaded regions defines the permitted domain of the secondary star in the log L–log $T_{\rm eff}$ diagram. This domain is shown as a hatched ellipse in Figure 8.

An essentially identical procedure was followed to define the domain of the primary star, with contour plots being created for each of the six adopted secondary temperatures (Casey 1996). For most secondary temperatures, the goodness-of-fit surface is again a valley along lines of approximately constant primary radius. The addition of the bolometric luminosity constraints again delimits more restricted regions for the primary star, and the union of these regions results in the trapezoidal region for the primary star shown in Figure 8.

We stress that with the data in hand we cannot select a single most probable solution for the primary and secondary of TY CrA. Numerous primary-secondary pairs along the center line of the secondary goodness-of-fit valley provide equally good fits to the light curve and satisfy the external constraints. Thus, the marked regions in Figures 7 and 8 should be taken as high confidence level boundaries for the primary and secondary stars rather than as normally distributed uncertainty domains about a particular solution. Furthermore, the derived physical parameters of the two stars are strongly correlated. Figure 7 should be used to derive the physical parameters of the secondary star for a given primary effective temperature.

The derived photometric elements are presented in Table 4. The radii are given relative to the orbital semimajor axis. The luminosity ratio is given only for the y band. Most of the values listed are the median values for the permitted ranges of each parameter, with the uncertainties showing the full range. The exceptions are the period and phase zero point (Min I), for which the uncertainties are standard deviations (§ 5.1), and the orbital eccentricity, which is adopted to be zero based on the spectroscopic orbital solutions.

Finally, we have checked that these solutions are consistent with the *uvb* data. The tertiary third-light contributions

[2] The fragmented structure of the 0.0073 mag contour along the goodness-of-fit valley in Fig. 7 is an artifact of the contouring routine and the limited number of grid points. Thus, we have smoothed over the circular features in defining the valley of acceptable solutions.

TABLE 4

PHOTOMETRIC ELEMENTS

Parameter	Median and Range
Period (days)	2.888779 ± 0.000013
Min I (JD)	2,449,537.8414 ± 0.0008
Eccentricity	0[a]
Inclination (deg).....	83 ± 1
r_{pri}	0.125 ± 0.007
r_{sec}	0.145 ± 0.010
$r_{pri} + r_{sec}$	0.272 ± 0.004
r_{pri}/r_{sec}	0.86 ± 0.15
l_{sec}/l_{pri} (y band)	0.085 ± 0.055

[a] Adopted.

in these bandpasses are not known, and the assumption that the luminosity ratio l_3/l_2 is the same as that derived at 6400 Å becomes increasingly poor toward the blue. Hence, for each of these bandpasses, the physical parameters (radii, temperatures, inclination) from the y solution were adopted and initially held fixed. The third-light parameter L_3 was then freed and a light-curve solution derived. The values found for L_3 were 0.59, 0.57, 0.54, and 0.50 for u, v, b, and y, respectively, showing the increasing influence of the nebular contribution for shorter wavelengths (see Table 2). These third-light parameters were then adopted and held fixed while the stellar parameters were freed and new light-curve solutions run. The derived stellar parameters were then compared with those obtained from the y solution. For each bandpass the derived stellar parameters were consistent with those derived from the y-band data.

6.3. *Absolute Dimensions*

The physical parameters for the primary and secondary stars of TY CrA are given in Table 5. Again, the values listed are the median values for the permitted ranges of each parameter, and the uncertainties defining the full range should be taken as high confidence level limits.

With the determination of the inclination angle, the binary orbit is fully specified. The stellar masses are 3.16 ± 0.02 and $1.64 \pm 0.01\ M_\odot$. The radii of both stars are similar: $R_1 = 1.8 \pm 0.10\ R_\odot$ and $R_2 = 2.08 \pm 0.14\ R_\odot$. Both fit comfortably within their Roche radii. The secondary has a temperature of $\approx$4900 K, making it a late G to early K spectral type. These physical parameters place the primary star of TY CrA near the zero-age main sequence, and the PMS secondary near the base of its Hayashi track, as can be seen by comparison with the evolutionary tracks from Swenson et al. (1994; F. J. Swenson 1995, private communication) shown in Figure 8. A detailed comparison of the TY CrA stars with theoretical tracks is taken up in § 7.

TABLE 5

PHYSICAL PARAMETERS

Parameter	Primary	Secondary
Stars:		
Mass ($M_\odot$)	3.16 ± 0.02	1.64 ± 0.01
Radius ($R_\odot$)	1.80 ± 0.10	2.08 ± 0.14
log g (cgs)	4.43 ± 0.06	4.02 ± 0.05
Temperature (K).....	12000 ± 500	4900 ± 400
Luminosity ($L_\odot$).....	67 ± 12	2.4 ± 0.8
v_{synch} (km s^{-1})	30 ± 5	36 ± 7
Binary:		
K (km s^{-1})[a]	85.2 ± 0.4	164.6 ± 1.6
a (AU)	0.0665 ± 0.0004	
a ($R_\odot$).....	14.29 ± 0.09	
d (pc).....	129 ± 11	

NOTES.—The light-curve analysis does not favor a single set of stellar parameters. The values given here delimit high confidence level ranges on the parameters and the median value of this range. Some parameters are strongly correlated within the ranges. (See § 6.)

[a] Paper II.

Interestingly, the convective atmosphere predicted for the secondary is supported by the fact that the bolometric albedo for the secondary always converged to values close to the theoretically expected value for stars with convective atmospheres (Vaz & Nordlund 1985; Nordlund & Vaz 1990). The mean bolometric albedo for the accepted solutions was 0.66 ± 0.08.

Finally, if we adopt an extinction of $A_V = 3.1$ mag (Cardelli & Wallerstein 1989), then the derived distance is 129 ± 11 pc. This is equal to the distance of 129 pc derived by Marraco & Rydgren (1981) for the R CrA dark cloud from spectroscopic parallaxes of three stars but is smaller than the distance of 242 pc they derive for TY CrA specifically, and which they consider to be suspect.

7. DISCUSSION

7.1. *Comparison with Previous Observations*

Bibo et al. (1992) and Paper I derive bolometric luminosities for TY CrA via spectroscopic parallaxes. These results (plotted in Fig. 7 of Paper II) show TY CrA lying above the zero-age main sequence (ZAMS) and above the region shown for the primary in Figure 8. However, these studies are based on photometric data that are not corrected for nebular light contributions. For example, the V observations in Kilkenny et al. (1985) used by Bibo et al. were obtained within diaphragm diameters of 21″–25″ (D. Kilkenny 1995, private communication). As discussed in § 2.2, we find that for a 17″ diaphragm the nebula contributes about 30% of the observed light at V. Analysis of our CCD images indicates that with a 25″ diaphragm the nebula would contribute about 40% of the light at V. If we decrease the Bibo et al. (1992) luminosity determinations by 40%, the (combined light) luminosity (49–59 $L_\odot$) agrees better with the values derived here. The measurements plotted in Paper II should likewise be lowered by about 40%.

7.2. *Comparison with Theoretical Models*

We have chosen to compare our results with three sets of theoretical PMS evolutionary models, specifically, Swenson et al. (1994), Claret (1995), and D'Antona & Mazzitelli (1994). The first two were chosen because we have models for several different chemical compositions, as well as tracks calculated for the specific masses of the primary and secondary stars. The D'Antona & Mazzitelli tracks are often used in studies of T Tauri stars. Here we test them against the PMS secondary star, exploring the effects of different opacity and convection theories.

Our analysis with the models of Swenson et al. is organized according to the precision with which we know the physical properties of the TY CrA stars. The stellar masses are precisely known (<1%) as a result of the high-quality radial velocity curves of Papers I and II and the weak dependence of mass on inclination angle at high inclinations. The stellar radii are also reasonably well deter-

mined (5%), as they are derived primarily from the duration of the eclipses. The temperatures of the primary and secondary are least well determined (5%–10%).

7.2.1. *Swenson et al. (1994)*

F. J. Swenson has kindly computed PMS evolutionary models for the specific masses of the TY CrA stars—3.16 $M_\odot$ and 1.64 $M_\odot$. As the chemical composition of the TY CrA system is unknown, models were computed with both solar ($X = 0.7098$, $Y = 0.2729$, $Z = 0.0173$) and Hyades ($X = 0.7160$, $Y = 0.2590$, $Z = 0.0250$) compositions. The code used is described in Swenson et al. (1994), with some subsequent updates.

In Figure 9, we compare observation and theory in the log g versus log ($M/M_\odot$) plane. Since the masses are well determined, comparison in log g is essentially a test of stellar radius. The filled squares and error bars represent the parameters derived for the primary and secondary of TY CrA (§ 6.3). The open squares represent predictions of the theoretical models of Swenson et al. (1994) at various ages; primary and secondary points of the same age are connected by lines. The solar and Hyades compositions are shown in the left and right panels, respectively. At an age of 3 Myr, the higher mass primary has reached the ZAMS. After 30 Myr, the secondary has still not quite reached the ZAMS, while the primary has already left the ZAMS and is again increasing in size (decreasing in log g).

The observational parameters for the primary star are consistent with theoretical ZAMS models of solar composition. The range in log g permitted for the primary star includes slightly pre–main-sequence models, with ages somewhat younger than 3 Myr, to slightly post–main-sequence models, with ages as large as 30 Myr. For the higher metallicity Hyades models the ZAMS radius is larger and, consequently, falls at lower log g than the primary star. A ZAMS model of Hyades composition is at best marginally consistent with the largest permitted radius for the primary star. The age of such a ZAMS model is roughly 10 Myr.

The secondary star is consistent with models of both solar and Hyades composition with ages of 3–10 Myr. For both compositions, log g of the secondary is far lower than that of the ZAMS models, clear evidence that the secondary star is still contracting toward the ZAMS. For solar-composition models the primary star is also consistent with the theoretical models throughout this age range.

Having found models that match the observed masses and radii of coeval primary and secondary stars, we now compare the observed and theoretical effective temperatures. In Figure 10 we plot log g versus log $T_{\rm eff}$. The solid and dashed curves are the theoretical evolutionary tracks for solar and Hyades compositions, respectively, again calculated for the masses of the TY CrA stars. The filled squares and error bars show the ranges of acceptable log g and log $T_{\rm eff}$ for the primary and secondary stars (see § 6.3 and Table 5). The open squares and triangles indicate locations at model ages of 3 and 10 Myr, respectively.

While the log g derived for the primary star is consistent with ZAMS models of solar composition, the observed effective temperature of the primary (12,000 $\pm$ 500 K; § 3) is cooler than the ZAMS temperature by 1100 K. The effective temperatures of the Hyades-composition tracks near the ZAMS are marginally consistent with the observed primary effective temperature.

The effective temperature of the secondary is consistent with both tracks. The higher temperatures of the solar-composition tracks are only consistent with light-curve solutions that have a high-temperature primary (e.g., 12,500 K; Fig. 7). Both the gravity and effective temperature of the secondary are best matched with theoretical models of

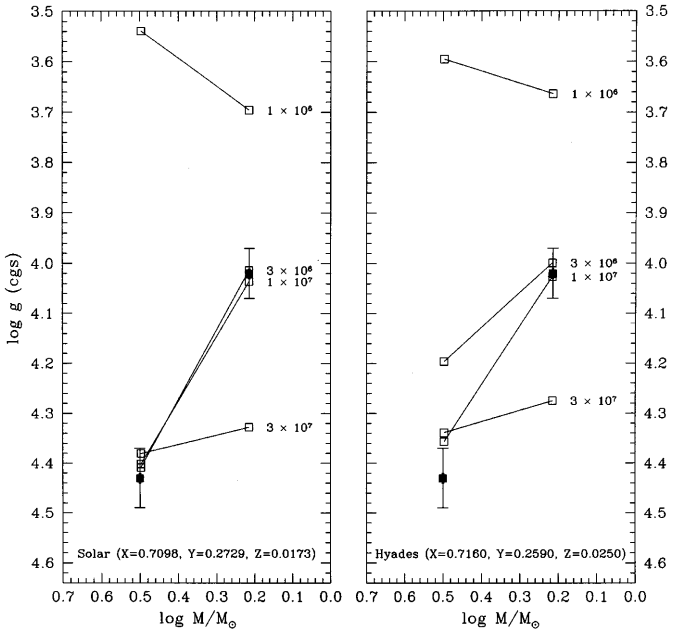

FIG. 9.—Comparison of theoretical models (Swenson et al. 1994) with the primary and secondary stars of TY CrA in the log g–log M plane. Filled squares with error bars mark the allowed regions for the primary and secondary stars. Open squares represent models at the indicated evolutionary times. The left panel is for models calculated with solar composition. The Hyades composition was used for models in the right panel.

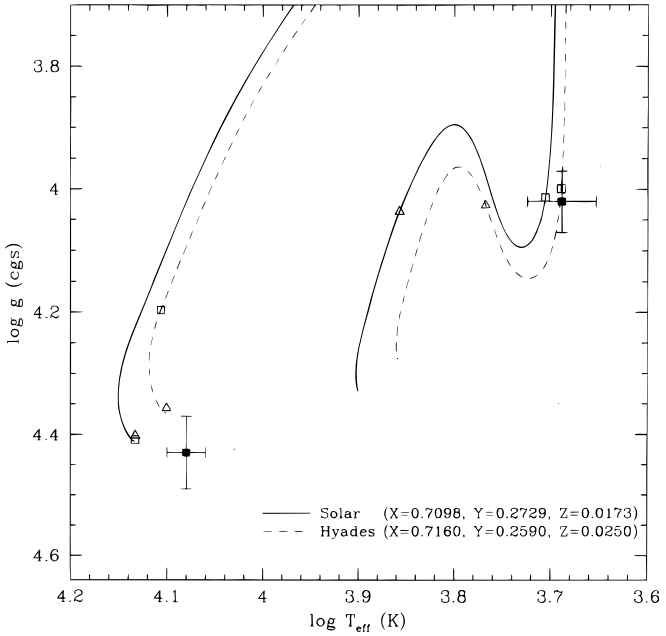

FIG. 10.—Comparison of theoretical models (Swenson et al. 1994) and the primary and secondary of TY CrA in the log g–log $T_{\rm eff}$ plane. Solid and dashed curves correspond to evolutionary tracks with solar and Hyades compositions, respectively. Filled squares with error bars mark the allowed regions for the primary and secondary stars. Open squares and triangles mark model points at ages of 3 and 10 Myr, respectively.

either composition having ages of order 3 Myr. Furthermore, the morphology of the tracks requires that the age not be substantially older than this. While the derived log g for the secondary is consistent with ages between 3 and 10 Myr (because of the turnaround in radius at the base of the Hayashi track), models with ages of 10 Myr already have effective temperatures significantly larger than observed for the secondary star. Thus, the addition of the temperature constraint has reduced the ambiguity in the age of the system that remained after the log g analysis.

However, for the Hyades-composition models the tight constraint on the secondary age produces a significant inconsistency in the primary radius. Assuming that the two stars are coeval, the theory predicts that a Hyades-composition primary would still be contracting to the main sequence with log g about 0.2 lower than on the ZAMS and even more deviant from the observed value. The solar-composition models do not have this difficulty; by an age of 3 Myr the theory predicts that the primary will have reached the main sequence and have a radius consistent with the observed primary radius. However, as noted, the solar-composition models predict a primary temperature significantly higher than observed.

Finally, in Figure 8 we show the locations of the primary and secondary stars of TY CrA and the Swenson evolutionary tracks in the theoretical H-R diagram. Again, the solid and dashed curves are for solar and Hyades compositions, respectively, and the squares and triangles indicate locations at model ages of 3 and 10 Myr, respectively. The dotted lines are drawn at constant values of radius.

The permitted region for the secondary star agrees well with models of either solar or Hyades compositions at an age of about 3 Myr. At this age, the secondary is still *pre–main sequence* and at the base of the Hayashi track. However, the permitted region for the primary star does not match either of the theoretical tracks. While the primary radius is consistent with that of a solar-composition ZAMS star, the effective temperature is significantly cooler than predicted by that track. The ZAMS position of a track with Hyades composition better matches the effective temperature of the primary star, but has a radius that is marginally too large. More problematic for the Hyades tracks, a primary that is *coeval* with the secondary has a radius that is much larger than that derived for the primary star. Thus, while the secondary star is consistent with the Swenson theoretical models, the primary star is not.

7.2.2. *Claret (1995)*

From Claret (1995; A. Claret 1995, private communication) we have theoretical PMS evolutionary tracks, again calculated for the masses of TY CrA but providing a larger range in helium and metal abundance. In Figure 11, we plot log g versus log $(M/M_{\odot})$; symbols are as in Figure 9. The trend of lower ZAMS log g with decreasing metallicity is repeated here. However, when compared with the Claret tracks the primary is *not* consistent with solar

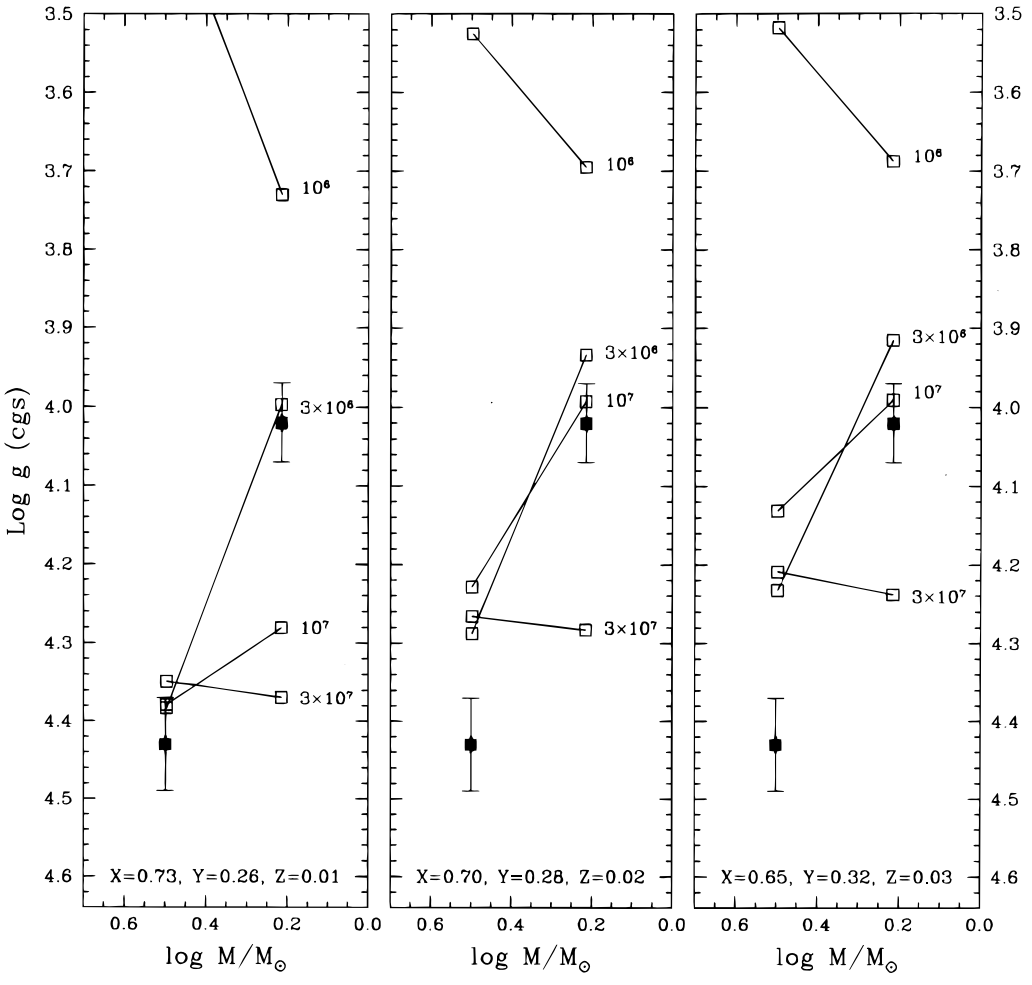

FIG. 11.—Same as Fig. 8, but showing theoretical models of Claret (1995) for three different compositions

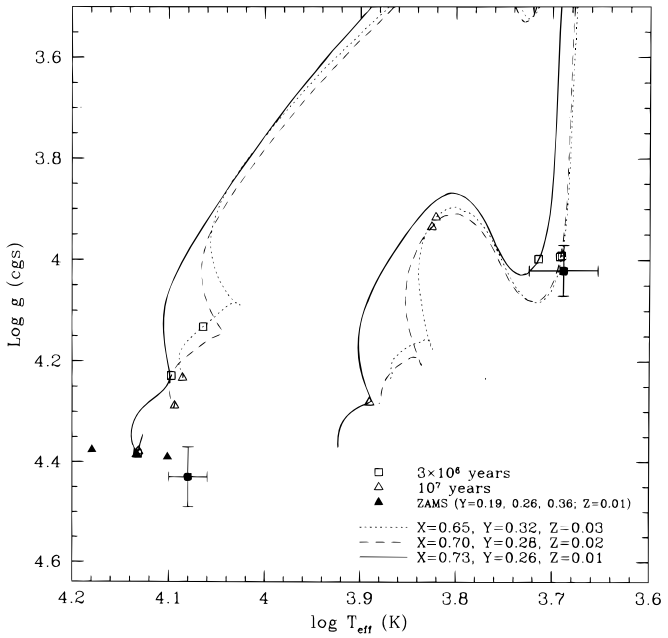

FIG. 12.—Comparison of theoretical models (Claret 1995) with the primary and secondary stars of TY CrA in the log g–log $T_{\rm eff}$ plane. The solid, dashed, and dotted tracks represent compositions with $Z = 0.01$, 0.02, and 0.03, respectively. Filled squares with error bars designate the acceptable regions for the primary and secondary stars. The filled triangles are drawn at ZAMS positions for the primary star for models with $Z = 0.01$ and $Y = 0.19$, 0.26, and 0.36, with higher He abundances corresponding to lower temperatures.

($Z = 0.02$) composition ZAMS models, in the sense that the observed radius is smaller than the theoretical radius. The primary star only agrees with lower metallicity ($Z = 0.01$) ZAMS models, and even then the agreement is marginal.

The secondary star is again consistent with all compositions. At the lower metallicity, where theoretical models can match both the primary and secondary stars, the only coeval solution is at an age of 3 Myr. At solar and higher metallicities an age of order 10 Myr is required for the secondary, although no solutions exist for both the primary and secondary stars.

To incorporate effective temperatures into the analysis, we plot log g versus log $T_{\rm eff}$ in Figure 12. The solid, dashed, and dotted curves represent Claret evolutionary tracks through an age of 30 Myr with $Z = 0.01$, 0.02, and 0.03, respectively. As before, only the $Z = 0.01$ track reaches a gravity as large as observed for the primary star. However, the $Z = 0.01$ ZAMS model predicts a higher effective temperature for the primary star than observed, similarly to the Swenson tracks.

We have used the Claret tracks to explore the impact of helium abundance on this effective temperature discrepancy. The filled triangles in Figure 12 mark the ZAMS locations of the $Z = 0.01$ models for helium abundances of $Y = 0.19$, 0.26, and 0.36, with lower He abundances producing higher effective temperatures. Consistency in effective temperature between the theoretical models and the observed primary star is achieved only for helium abundances exceeding $Y = 0.36$.

The primary star is thus again inconsistent in effective temperatures with theoretical tracks of typical compositions. The discrepancy can be resolved by raising the helium abundance, but the required value, in excess of $Y = 0.36$, seems implausible. The effective temperature of the secondary star matches both the solar and higher metallicity models; it is only marginally consistent with the low-metallicity ($Z = 0.01$) model. In the case of the Claret models, this further hinders a self-consistent solution for both the primary and secondary stars.

7.2.3. *D'Antona & Mazzitelli (1994)*

The tracks of D'Antona & Mazzitelli (1994) have frequently been used to assign masses and ages in recent studies of PMS stars. The available tracks do not extend to as high mass as the primary of TY CrA, but they do permit comparison with the PMS secondary star. Hence we restrict our analysis to the secondary star and explore the effects of different opacities and convection models on the comparison.

The permitted domain of the secondary star in the theoretical H-R diagram is shown by the hatched regions in Figure 13. Also shown are the evolutionary tracks (*solid curves*) and isochrones (*dotted lines*) of D'Antona & Mazzitelli (1994), computed with solar composition. The four panels of the figure represent combinations of two opacities and two models of convection. The "Alexander" opacities are from Alexander, Augason, & Johnson (1989), supplemented with values from Rogers & Iglesias (1992) and Huebner et al. (1997). The "Kurucz" opacities are those of Kurucz (1991), supplemented with values from Rogers & Iglesias. The convection models are the standard mixing-length theory (MLT; Böhm-Vitense 1958) and that of Canuto & Mazzitelli (1990, 1992). The dashed evolutionary track corresponds to a 1.64 $M_\odot$ star, derived by interpolating between the 1.6 $M_\odot$ and 1.8 $M_\odot$ tracks. Also shown are isochrones (*dotted lines*) at ages of 1, 3, and 10 Myr, from top right to bottom left, respectively.

The permitted domain for the secondary star includes the 1.64 $M_\odot$ theoretical tracks of all four models. As with the Swenson et al. (1994) models, the relatively high minimum luminosities of these solar-composition tracks ($\log L > 0.35$) are only consistent with solutions for TY CrA that have higher temperature primary stars (e.g., 12,500 K; Fig. 7). The MLT models pass centrally through the permitted domain for the secondary star and match several excellent light-curve solutions for the TY CrA system. However, the higher luminosities and temperatures of the models employing Canuto-Mazzitelli convection only match more marginal light-curve solutions (see Fig. 7), particularly in the case of Alexander opacities. While it would be premature to rule out Canuto-Mazzitelli convection, our light-curve solutions for the TY CrA secondary are better matched by the MLT models.

The intersection of the 1.64 $M_\odot$ tracks and the observed parameters for the secondary star indicate an age of about 3 Myr for all of the models, as also derived from the Swenson et al. (1994) and Claret (1995) tracks.

8. SUMMARY AND CONCLUSIONS

We have presented a detailed analysis of new light-curve observations of the eclipsing triple system TY CrA. The shallow (3% depth) secondary eclipse is securely detected. The system also shows noneclipse luminosity variations on timescales from days to years. Together with our spectroscopic limits on the luminosity ratio, analysis of the light curve provided physical parameters for the primary and secondary stars. The stellar masses are $M_1 = 3.16 \pm 0.02$ $M_\odot$ and $M_2 = 1.64 \pm 0.01$ $M_\odot$, respectively. The stellar

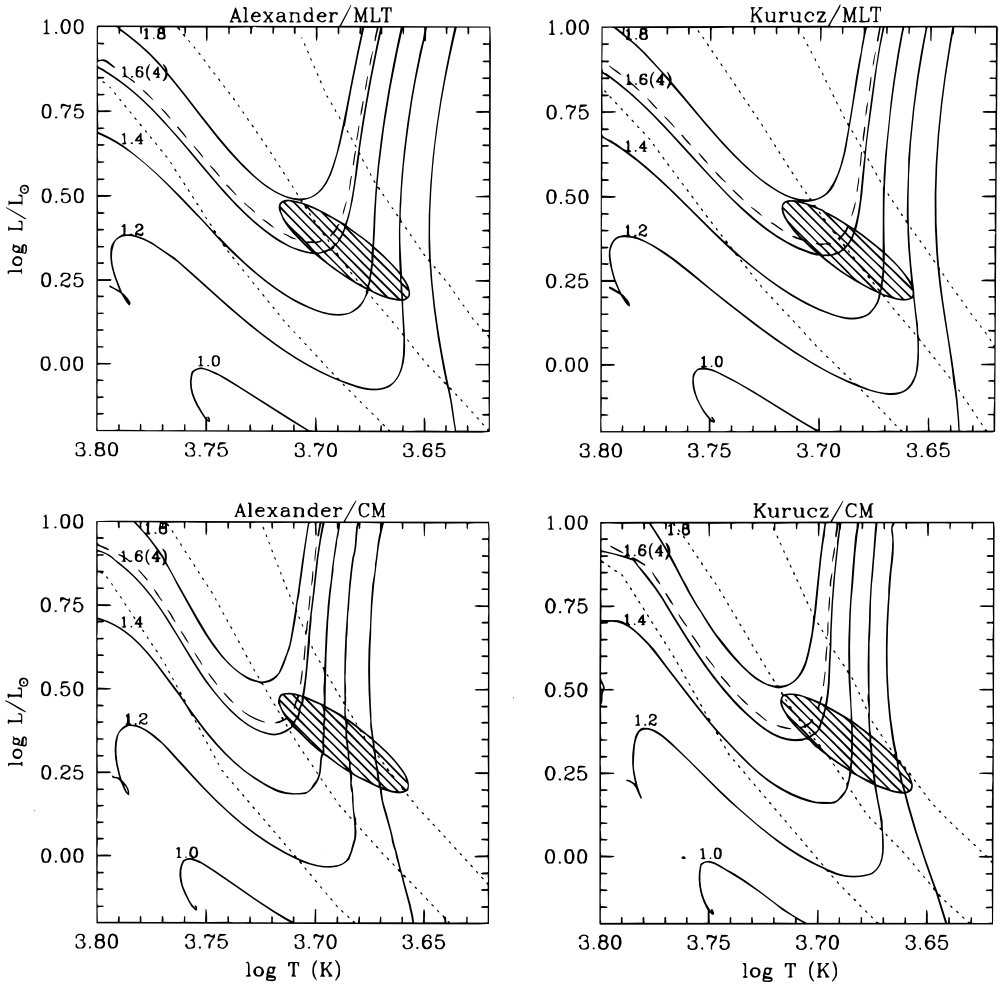

FIG. 13.—Theoretical H-R diagrams centered on the secondary of TY CrA. The solid curves are pre–main-sequence evolutionary tracks from D'Antona & Mazzitelli (1994). The dashed curve corresponds to a 1.64 $M_\odot$ track, derived by interpolating between the 1.6 $M_\odot$ and 1.8 $M_\odot$ tracks. Dotted lines are isochrones drawn at 1, 3, and 10 Myr. The hatched ellipse is the high-confidence domain based on light-curve analyses. The four panels show different combinations of opacities and convection models, as labeled (see § 6.2).

radii are $R_1 = 1.8 \pm 0.1\ R_\odot$ and $R_2 = 2.08 \pm 0.14\ R_\odot$, respectively. Adopting a temperature of 12,000 $\pm$ 500 K for the primary star from photometric and spectral type information, we derive a temperature of 4900 $\pm$ 400 K for the secondary star. The stellar luminosities are $L_1 = 67 \pm 12\ L_\odot$ and $L_2 = 2.4 \pm 0.8\ L_\odot$, respectively. Here the uncertainties represent high-confidence limits, not standard deviations. Finally, we note that the secondary radius of $R_2 = 2.08 \pm 0.14\ R_\odot$ corresponds to a synchronous rotational velocity of 32 ± 6 km s^{-1}, consistent with the observed value of $v \sin i = 36 \pm 7$ km s^{-1} (Paper II).

The large radius of the secondary star, along with its association with the R CrA dark cloud and lithium absorption (Paper II), identify it as pre–main sequence. Comparison with theoretical models places it consistently at the base of the Hayashi track, with an age of 3 Myr. As such, the secondary star of TY CrA is the youngest pre–main-sequence star with a well-determined mass and radius, and the first opportunity to directly test the mass calibration of Hayashi tracks. We have compared the secondary star with three sets of solar-composition theoretical tracks—Swenson et al. (1994), Claret (1995), and D'Antona & Mazzitelli (1994). In all three cases, solar-composition 1.64 $M_\odot$ tracks are consistent with the observed physical parameters given a higher temperature primary star (e.g., 12,500 K). Thus, at the most basic level these results support the use of pre–main-sequence evolutionary tracks for the interpretation of T Tauri stars and suggest that the mass calibrations of modern tracks are reasonable. In detail, higher metallicity compositions are also consistent with the TY CrA secondary; however, lower metallicity models tend to be hotter than the observed stellar properties. In the case of the D'Antona & Mazzitelli models, mixing-length theory models provide marginally better matches than models employing Canuto-Mazzitelli convection theory, at least for solar composition.

On the other hand, comparison of evolutionary tracks for the near-ZAMS primary star with the observations leads to puzzling results. First, we note that for given composition and mass, the Swenson et al. ZAMS models have smaller radii than the Claret models. As a consequence, the Swenson et al. model radii are consistent with the observed radius for the primary for both solar and (marginally) Hyades compositions, but an acceptable fit for the Claret models is only possible for a metallicity about half that of the Sun. While such a low metallicity has some precedent, both in binary and field stars (Andersen, Clausen, & Giménez 1993; Gies & Lambert 1992), it does aggravate the second—and independent—discrepancy with both sets of models: the derived effective temperature of the primary

star is approximately 1000 K cooler than theoretical ZAMS temperatures for a solar-composition 3.16 $M_\odot$ star. This discrepancy is not resolvable through variations in composition unless an implausibly high helium abundance ($Y = 0.36$) is adopted (see also Casey 1996).

It is interesting to reflect whether the refusal of the primary of TY CrA to conform to conventional single-star models might be linked to its other most outstanding peculiarity, its very sharp-lined spectrum. The latter suggests that the photosphere rotates far below the synchronous velocity firmly expected for the short period and circular orbit of TY CrA (Paper I; Lagrange et al. 1993). An essentially nonrotating star in such a binary system is observationally unique, yet the spectrum shows no sign of a nonphotospheric origin. In searching for a plausible physical explanation, it may be relevant to note that rapid internal rotation moves a star downward and nearly parallel to the nonrotating main sequence in the H-R diagram, similar to the position of the TY CrA primary with respect to the theoretical models (Law 1981). Perhaps the interior of the TY CrA primary is in fact rapidly rotating (as expected for a late B star), while the surface has been braked by a magnetic wind. While entirely ad hoc, this conjecture could explain the TY CrA primary.

The consistency of the TY CrA secondary with pre–main-sequence evolutionary tracks is an encouraging result for pre–main-sequence theory, being the first direct test of the mass calibration of Hayashi tracks. Nonetheless, the secondary of TY CrA is only one case, and the uncertainties in the secondary temperature and composition did not permit adequately critical tests of different theoretical tracks. Furthermore, both stars of TY CrA presumably had substantially larger radii earlier in their evolution. Depending on the details of the system's previous orbital evolution, it is possible that the system has not always been detached; consequent implications for the evolution of the two stars should be considered. From an observational perspective, more precise determinations of the stellar parameters of TY CrA and other similarly young stars are necessary to significantly constrain the physics of pre–main-sequence evolutionary theory.

We thank F. Swenson, F. D'Antona, A. Claret, and D. VandenBerg for providing their theoretical models in digital form and for calculating some models specifically for this work. We also acknowledge D. VandenBerg for pointing out the possible link between rotation and the cool temperature of the primary star. We thank D. Kilkenny for searching old observational logs. B. W. C. acknowledges support from the Wisconsin Alumni Research Foundation and the Wisconsin Space Grant Consortium. R. D. M. acknowledges support from a Presidential Young Investigator award and NSF grant AST 94-1715. J. A. received support from the Danish Natural Science Research Council, the Danish Board for Astronomical Research, and the Carlsberg Foundation. This research has made use of the SIMBAD database, operated at CDS, Strasbourg, France.

REFERENCES

Alencar, S. H. P., & Vaz, L. P. R., 1997, A&A, 326, 257
Alexander, D. R., Augason, G. C., & Johnson, H. R. 1989, ApJ, 1014
Andersen, J. 1991, A&A Rev., 3, 91
Andersen, J., Clausen, J. V., & Gimenénez, A. 1993, A&A, 277, 439
Beust, H., Corporon, P., Siess, L., Forestini, M., & Lagrange, A.-M. 1997, A&A, 320, 478
Bibo, E. A., Thé, P. S., & Dawanas, D. N. 1992, A&A, 260, 293
Böhm-Vitense, E. 1958, Z. Astrophys., 46, 108
Buser, R., & Kurucz, R. L. 1992, A&A, 264, 557
Canuto, V. M., & Mazzitelli, I. 1990, ApJ, 370, 295
———. 1992, ApJ, 389, 724
Cardelli, J. A., & Wallerstein, G. 1989, AJ, 97, 1099
Casey, B. W. 1996, Ph.D. thesis, Univ. Wisconsin–Madison
Casey, B. W., Mathieu, R. D., Suntzeff, N. B., Lee, C. W., & Cardelli, J. A. 1993, AJ, 105, 2276 (Paper I)
Casey, B. W., Mathieu, R. D., Suntzeff, N. B., & Walter, F. M. 1995, AJ, 109, 2156 (Paper II)
Claret, A. 1995, A&A, 109, 441
Claret, A., Giménez, A., & Martín, E. L. 1995, A&A, 302, 741
Corporon, P., Lagrange, A. M., & Beust, H. 1996, A&A, 310, 228
Corporon, P., Lagrange, A. M., & Bouvier, J. 1994, A&A, 282, L21
D'Antona, F., & Mazzitelli, I. 1994, ApJS, 90, 467
Davis, J. & Shobrook, R. R. 1977, MNRAS, 178, 651
Eddington, A. S. 1926, MNRAS, 86, 320
Ghez, A. M., Weinberger, A. J., Neugebauer, G., Matthews, K., & McCarthy, D. W., Jr. 1995, AJ, 110, 753
Gies, D. R., & Lambert, D. L. 1992, ApJ, 387, 673
Herbig, G. H., & Rao, N. K. 1972, ApJ, 174, 401
Herbst, W., Herbst, D. K., Grossman, E. J., & Weinstein, D. 1994, AJ, 108, 1906
Hillenbrand, L. A., Strom, S. E., Vrba, F. J., & Keene, J. 1992, ApJ, 397, 613
Huebner, W. F., Merts, A., Magee, N. F., & Argo, M. F. 1977, Astrophysical Opacity Library (Rep. LA-6760-M) (Los Alamos: Los Alamos Sci. Lab.)
Kardopolov, V. I., Sahanionok, V. V., & Philipjev, G. K. 1981, Perem. Zvezdy, 21, 589
Kilkenny, D., Whittet, D. C. B., Davies, J. K., Evans, A., Bode, M. F., Robson, E. I., & Banfield, R. M. 1985, South African Astron. Obs. Circ., 9, 55
Kurucz, R. L. 1979, ApJS, 40, 1
Kurucz, R. L. 1991, in Stellar Atmospheres: Beyond Classical Models, ed. L. Crivellari, I. Hubeny, & D. G. Hummer (NATO ASI Ser. C, 341) (Dordrecht: Kluwer), 441
Kwee, K. K., & van Woerden, H. 1956, Bull. Astron. Inst. Netherlands, 12, 327
Lafler, J., & Kinman, T. D. 1965, ApJS, 11, 216
Lagrange, A.-M., Corporon, P., & Bouvier, J. 1993, A&A, 274, 785
Law, W.-Y. 1981, A&A, 102, 178
Lucy, L. B. 1967, Z. Astrophys., 65, 89
Marraco, H. G., & Rydgren, A. E. 1981, AJ, 86, 62
Martín, E. L., & Rebolo, R. 1993, A&A, 274, 274
Napiwotzki, R., Schönberner, D., & Wenske, V. 1993, A&A, 268, 653
Nielsen, R. F., Nørregaard, P., & Olsen, E. H. 1987, Messenger, 50, 45
Nordlund, Å., & Vaz, L. P. R. 1990, A&A, 228, 231
Popper, D. M. 1980, ARA&A, 18, 115
———. 1987, ApJ, 313, L81
Rogers, F. J., & Iglesias, C. A. 1992, ApJS, 79, 507
Shobbrook, R. R. 1976, MNRAS, 176, 673
Straizys, V., & Kuriliene, G. 1981, Ap&SS, 80, 353
Swenson, F. J., Faulkner, J., Roger, F. J., & Iglesias, C. A. 1994, ApJ, 425, 286
Van Hamme, W. 1993, AJ, 106, 2096
Vaz, L. P. R. 1984, Ph.D. thesis, Copenhagen Univ. Obs.
———. 1986, Rev. Mexicana Astron. Astrofis., 12, 177
Vaz, L. P. R., Andersen, J. & Rabello Soares, M. C. A. 1995, A&A, 301, 693
Vaz, L. P. R., Andersen, J., Casey, B. W., Clausen, J. V., Mathieu, R. D., & Heyer, I. 1998, A&AS, in press
Vaz, L. P. R., & Nordlund, Å. 1985, A&A, 147, 281
Vitrichenko, E. A., & Shevchenko, V. S. 1995, AZh Pisma, 21, 434 (English transl. Astron. Lett., 21, 386) (VS)
von Zeipel, H. 1924, MNRAS, 84, 665
Wilson, R. E. 1993a, Documentation of Eclipsing Binary Computer Model (revision of 1992 May, updated 1993 January)
———. 1993b, in ASP Conf. Ser. 38, New Frontiers in Interacting Binary Star Research, ed. K.-C. Leung & I.-S. Nha (San Francisco: ASP), 91
Wilson, R. E., & Devinney, E. J. 1971, ApJ, 166, 605
Wood, D. B. 1971, AJ, 76, 701
———. 1972, A Computer Program for Modeling Non-spherical Eclipsing Binary Systems (Greenbelt, MD: GSFC)